

Effect of system level structure and spectral distribution of the environment on the decoherence rate ^{*}

Jingfu Zhang, Xinhua Peng, Nageswaran Rajendran, and Dieter Suter

Fachbereich Physik, Universität Dortmund,

44221 Dortmund, Germany

(Dated: July 14, 2018)

Abstract

Minimizing the effect of decoherence on a quantum register must be a central part of any strategy to realize scalable quantum information processing. Apart from the strength of the coupling to the environment, the decoherence rate is determined by the the system level structure and by the spectral composition of the noise trace that the environment generates. Here, we discuss a relatively simple model that allows us to study these different effects quantitatively in detail. We evaluate the effect that the perturbation has on a nuclear magnetic resonance (NMR) system while it performs a Grover search algorithm.

PACS numbers: 03.67.Lx

^{*} Corresponding authors: Jingfu Zhang, zhangjfu2000@yahoo.com, Jingfu@e3.physik.uni-dortmund.de; Dieter Suter, Dieter.Suter@uni-dortmund.de

I. INTRODUCTION

The advantage that quantum computers have over classical computers hinges on the creation and preservation of quantum coherence [1]. Any real quantum computer, however, interacts with its environment and such interactions result in decoherence which increases the probability that the quantum computation may fail [2]. Decoherence is thus one of the main obstacles for building practical quantum computers.

A number of strategies have developed for suppressing decoherence, including quantum error corrections [3], dynamical decoupling (quantum control) [4], decoherence-free subspaces [5], holonomic quantum computation [6], the quantum Zeno effect [7], and spectral degeneracy systems [8, 9]. It has been proved that the first four strategies can be unified under a general algebraic framework [10], and the quantum Zeno effect can be unified with dynamical decoupling [11]. Up to the present quantum error corrections [12], decoherence-free subspaces [13], holonomic quantum computation [14], and the suppression of artificial decoherence by dynamical decoupling (bang-bang control) [15] have been experimentally tested using nuclear magnetic resonance (NMR).

In this paper, we concentrate on a different aspect: The decoherence rate is not only determined by the strength of the coupling to the environment, but also by its operational form. As an example, the decoherence differs qualitatively if the coupling operator commutes with the system operator. Another aspect is the spectral composition of the noise: If the environment is (almost) static, the interaction is adiabatic. If it has components that fluctuate at transition frequencies of the system Hamiltonian, its effect can be particularly strong.

A number of model systems have been discussed to study the interaction of a quantum register with a noisy environment. One model is known as the spin bath where the environment consists of a set of two-level systems or spin-1/2 systems [16]. In another model, the so-called spin-boson model, the environment consists of a set of harmonic oscillators [17, 18, 19, 20]. NMR can simulate the decoherence effect (or called artificial decoherence) through the interactions generated by the spins viewed as spin bath [15, 21, 22] or implement error models by radio-frequency and gradient pulses for demonstrating quantum error corrections [12].

Here, we use a semiclassical model, where the environment acts on the system through

classical stochastic fields. The effect on the system is the same as that of other environments, provided a suitable ensemble average is taken. The coupling to the system occurs through spin operators. We distinguish two systems, in one of which the coupling operator commutes with the system Hamiltonian, in the other it does not. For both systems, we implement a Grover search algorithm[23, 24] and demonstrate the effect of different environments.

II. SYSTEM AND ENVIRONMENT

A. System Hamiltonian

We use a system of two qubits to compare the effect of different colored noise for different energy level structures. The Hamiltonian of the system is

$$H_s = \frac{1}{2}\hbar \left[\omega_z^1 \sigma_z^1 + \omega_z^2 \sigma_z^2 - \omega_x^2 \sigma_x^2 + \pi J \sigma_z^1 \sigma_z^2 \right]. \quad (1)$$

Here $\sigma_{x/z}^i$ denotes the x or z component of the Pauli matrix for spin i , $\omega_{x/z}$ describes the strength of the magnetic field along the x or z axis, respectively, and J denotes the coupling constant.

For suitable parameter sets, this Hamiltonian can execute a controlled NOT (CNOT) operation in a single step, without external control operations [9]; for a wider set of parameters, two-qubit gate operations can be executed that fall into the CNOT equivalence class, i.e. they are equivalent to the CNOT operation up to single qubit operations. Table I summarizes two parameter sets: System I (left hand column) gives the parameters for the CNOT operation, system II (right hand column) the parameters for a CNOT-equivalent operation. We write the Hamiltonians of the 2 systems H_s^I and H_s^{II} . Their eigenvalues are also shown in Table I. The transition angular frequencies are $\omega_{nm} = (E_n - E_m)/\hbar$ for each system, where $n, m = 1, 2, 3, 4$. The different energy level structures of the two systems provides the possibility to suppress decoherence induced by the coupling to the environment.

B. Coupling to the Bath

We now consider decoherence processes that are induced by a coupling to the environment that takes the form

$$H(t) = H_s + \hbar \pi s(t) A. \quad (2)$$

TABLE I: Parameters for the two systems in units of πJ , where J is the coupling constant.

	System I	System II
ω_z^1	0.378	0.378
ω_z^2	1	1
ω_x^2	2.272	1.136
E_1	$-1.32\hbar$	$-0.961\hbar$
E_2	$-1.32\hbar$	$-0.758\hbar$
E_3	$0.948\hbar$	$0.379\hbar$
E_4	$1.70\hbar$	$1.34\hbar$

For our purpose, the system operator A may be either σ_z^1 , σ_z^2 , or $\sigma_z^1 + \sigma_z^2$. The bath term $s(t)$ of the coupling operator may be either a classical random field or a quantum mechanical operator; for our purposes, it will be sufficient to consider it a time-dependent magnetic field with zero mean.

For the random perturbation $s(t)$, we consider stochastic functions with a Lorentzian spectral distribution of the power spectrum

$$S(\omega) = \frac{\kappa\Gamma}{\Gamma^2 + (\omega - \omega_0)^2} \quad (3)$$

and check the effect of the center frequency ω_0 on the decoherence rate in the two systems, where κ describes the strength of $S(\omega)$.

In the experiment, the coupling constant J had the value $J = 215 \text{ s}^{-1}$. To simulate the effect of the environment, we generated the stochastic functions by digital filtering of a random time series. Each time series had a duration of 24.35 ms consisted of 80 segments. For each time series we performed an experiment and summed over the individual experimental data. Figure 1 shows the power spectra of some time series $s(t)$ and the RMS spectral density $\sqrt{S(\omega)}$. Figure 2 shows the spectral density functions [25] for the four reservoirs that we compare, in relation to the transition frequencies of the system.

III. GROVER SEARCH IN NOISY SYSTEMS

The elementary gates in the Grover search are the Walsh- Hadamard transform and the controlled phase reversal $I_{|x\rangle}$ where $|x\rangle$ denotes a computational basis state, e.g. $|00\rangle$ or $|11\rangle$. $I_{|x\rangle}$ can be implemented by CNOT gates and one- qubit operations [19]. Hence we first implement the CNOT gate using the evolution under H_s (1).

A. Implementation of CNOT gates

As stated in the introduction, the system Hamiltonian generates a CNOT-equivalent operation without additional gate operations, i.e., for a suitable time t_C , $U(t) = e^{-it_C H_s/\hbar}$ becomes

$$C_e = C R_z^1(\phi),$$

where $R_z^1(\phi) = e^{i\phi\sigma_z^1/2}$ and

$$C = \begin{pmatrix} 1 & 0 & 0 & 0 \\ 0 & 1 & 0 & 0 \\ 0 & 0 & 0 & 1 \\ 0 & 0 & 1 & 0 \end{pmatrix}. \quad (4)$$

We diagonalise the Hamiltonian $H_s = V D V^\dagger$. Here, V represents the eigenvector matrix

$$V = \begin{pmatrix} \alpha_1 & \alpha_2 & 0 & 0 \\ \beta_1 & \beta_2 & 0 & 0 \\ 0 & 0 & \gamma_1 & \gamma_2 \\ 0 & 0 & \delta_1 & \delta_2 \end{pmatrix}, \quad (5)$$

and D is the diagonal form of the Hamiltonian, with eigenvalues

$$\lambda_{1,2} = \hbar\pi[\nu_z^1 \pm \sqrt{(\nu_x^2)^2 + (\nu_z^2 + \frac{J}{2})^2}]$$

$$\lambda_{3,4} = \hbar\pi[-\nu_z^1 \pm \sqrt{(\nu_x^2)^2 + (\nu_z^2 - \frac{J}{2})^2}].$$

To determine the required evolution time t_C , we choose the target operator as C_e and calculate the fidelity [26],

$$F(\phi, t) = |Tr[U(t)C_e^\dagger]|/4.$$

We find

$$F(\phi, t) = |e^{-it\lambda_1/\hbar} + e^{-it\lambda_2/\hbar} - \frac{\nu_x^2 e^{i\phi}}{\sqrt{(\nu_x^2)^2 + (\nu_z^2 - \frac{J}{2})^2}}(e^{-it\lambda_3/\hbar} - e^{-it\lambda_4/\hbar})|/4. \quad (6)$$

Numerical solutions for $J = 215 \text{ s}^{-1}$ are for system I $\phi_C^I = 0$, $t_C^I = 6.15 \text{ ms}$, resulting in $F > 0.9999$, and for system II $\phi_C^{II} = 0.18\pi$, $t_C^{II} = 4.05 \text{ ms}$, or $\phi_C^{II} = 0.52\pi$, $t_C^{II} = 12.18 \text{ ms}$, $F > 0.999$. Figure 3 shows the time dependence of the fidelity for the three cases.

B. Grover search

Using CNOT gates, one obtains the controlled phase reversal $I_{|11\rangle} = W^2 C W^2$ and $I_{|00\rangle} = e^{i(\pi/2)\sigma_z^{1,2}} I_{|11\rangle}$ where W^2 denotes the Walsh-Hadamard transform for qubit 2. The single-qubit gate operations required for the Grover algorithm are implemented by short radio-frequency pulses, whose duration is negligible compared to the two-qubit gate. It is therefore sufficient to consider the coupling to the reservoir during the evolution under H_s^I and H_s^{II} .

Including the perturbations, the total Hamiltonians are $H_k^I(t) = H_s^I + \hbar\pi\alpha s_k(t)A$ and $H_k^{II}(t) = H_s^{II} + \hbar\pi\alpha s_k(t)A$, respectively, where $s_k(t)$ has been normalized and α represents the strength of the perturbation. The perturbed Hamiltonian generates a perturbed phase reversal $\tilde{I}_{k,|x\rangle}$, which deviates slightly from the ideal operation $I_{|x\rangle}$, and which differs for each instance of $s_k(t)$.

The initial state for the Grover search is the uniform superposition $|\Psi_0\rangle = (|00\rangle + |01\rangle + |10\rangle + |11\rangle)/2$ obtained by applying $W^{1,2}$ to $|00\rangle$. We choose the target state as $|11\rangle$. Figure 4 shows the sequence of gate operations for the full Grover search algorithm $G = W^{1,2} I_{|00\rangle} W^{1,2} I_{|11\rangle}$ where we have used $W = W^{-1}$.

In system I the a single CNOT gate takes 6.09 ms, in the second system either 4.05 or 12.18 ms. To make the duration of the algorithm in both systems comparable, we replaced the second CNOT operation in system I by CNOT³, which takes 18.26 ms. Since the algorithm includes 2 CNOT gates, the total duration is close to 24 ms in both systems.

In each experiment, we start from the pseudo-pure state $|\Psi_0\rangle$. The perturbed Grover search $G_k = W^{1,2} \tilde{I}_{|00\rangle} W^{1,2} \tilde{I}_{|11\rangle}$ transforms it into $|\Psi_k\rangle = G_k |\Psi_0\rangle$ and the corresponding density matrix into $\rho_k = |\Psi_k\rangle\langle\Psi_k|$. Averaging over the individual signals gives the average (mixed) density matrix [27, 28]

$$\rho = \frac{1}{M} \sum_{k=1}^M \rho_k. \quad (7)$$

C. Decoherence during the search process

To quantify the loss of coherence by the environmental perturbation, we measured the purity of the Grover search process [29] by averaging the purity of the final states for proper input states. For this purpose, we chose a set of states that is uniformly distributed over the Bloch sphere. The uniformly distributed set of input states consists of the 36 states $|\Psi_{in}^{(n)}\rangle = |\psi_a\rangle|\psi_b\rangle$, ($a, b = 1, 2, \dots, 6$) where $|\psi_{a,b}\rangle \in \{|0\rangle, |1\rangle, (|0\rangle + |1\rangle)/\sqrt{2}, (|0\rangle - |1\rangle)/\sqrt{2}, (|0\rangle + i|1\rangle)/\sqrt{2}, (|0\rangle - i|1\rangle)/\sqrt{2}\}$.

The average purity for the algorithm is then $P = \frac{1}{36} \sum_{n=1}^{36} \text{Tr}\{[\rho^{(n)}]^2\}$ where $\rho^{(n)}$ denotes the output density matrix after completion of the quantum search for the input states $\rho_{in}^{(n)} = |\Psi_{in}^{(n)}\rangle\langle\Psi_{in}^{(n)}|$. Note that $|\Psi_0\rangle$ is one of the 36 input states.

When the systems are embedded in the reservoirs shown in Figure 2, the final states $\rho^{(n)}$ can be calculated by solving the Bloch- Redfield equations. In the eigenbase of the system Hamiltonian H_s in Eq. (1), the Bloch- Redfield equations are

$$\dot{\rho}_{nm} = -i\omega_{nm}\rho_{nm} - \sum_{k,l} R_{nmkl}\rho_{kl}. \quad (8)$$

where R_{nmkl} denotes the partial decoherence rates

$$R_{nmkl} = \delta_{lm} \sum_r \Lambda_{nrrk} + \delta_{nk} \sum_r \Lambda_{lrrm}^* - \Lambda_{lmnk} - \Lambda_{knml}^*. \quad (9)$$

Λ_{lmnk} denotes the element of the relaxation tensor. Eq. (9) shows that one can obtain R_{nmkl} through the real parts of the relaxation tensor represented as

$$\text{Re}\{\Lambda_{lmnk}\} = \frac{1}{4\pi} S(\omega_{nk})(A_{lm}A_{nk}). \quad (10)$$

When $A = \sigma_z^2$, it takes the form

$$A^I = \begin{pmatrix} 0 & 0 & -1 & 0 \\ 0 & -0.6606 & 0 & 0.7507 \\ -1 & 0 & 0 & 0 \\ 0 & 0.7507 & 0 & 0.6606 \end{pmatrix}, \quad A^{II} = \begin{pmatrix} -0.8695 & 0 & 0 & 0.4940 \\ 0 & 0 & -1 & 0 \\ 0 & -1 & 0 & 0 \\ 0.4940 & 0 & 0 & 0.8695 \end{pmatrix} \quad (11)$$

in the energy representation of the systems I and II, respectively. When $A = \sigma_z^1$, it is

diagonal because $[\sigma_z^1, H_s] = 0$. The matrices in the two systems are then

$$A^I = \begin{pmatrix} -1 & 0 & 0 & 0 \\ 0 & 1 & 0 & 0 \\ 0 & 0 & -1 & 0 \\ 0 & 0 & 0 & 1 \end{pmatrix}, \quad A^{II} = \begin{pmatrix} 1 & 0 & 0 & 0 \\ 0 & -1 & 0 & 0 \\ 0 & 0 & -1 & 0 \\ 0 & 0 & 0 & 1 \end{pmatrix}. \quad (12)$$

Eqs. (8-10) show that decoherence can be suppressed by choosing the parameters of H_s such that the elements of the tensor \mathbf{R} get small [8]. Qualitatively, the influence of the environment depends on the size of $|S(\omega_{nk})A_{nk}|$.

D. Numerical evaluation

We first present a numerical evaluation of Eq. (8) to calculate the purity $P_{1,2}$ for the two systems. Figures 5 and 6 summarize the result. Figures 5 (a-c) show the purity for the perturbation operator $A = \sigma_z^2$ and the reservoirs R1-R3. In Figure (a), the increase of α , has very little effect on P_2 because $S(\omega_{nk}^{II}) \approx 0$. However, P_1 decreases significantly, because $S(\omega_{42}^I)A_{42}^I = 0.7507$. Comparing the two systems in R1, one finds that system II is more robust. In Figure (5 b) the situation is reversed and system I is more robust. In Figure (5 c), P_1 decreases faster than P_2 because $|S(\omega_{31}^I)A_{31}^I| > |S(\omega_{41}^{II})A_{41}^{II}|$. These results illustrate the possibility to suppress decoherence by choosing an appropriate energy level structure.

When $A = \sigma_z^1$, it is diagonal in the eigenbase of the Hamiltonian. In this case, the reservoir does not induce transitions, but only causes dephasing, according to Eq. (12). The energy level structure has then only a small effect on the decoherence rates. From Eq. (10), one finds that the reservoir affects the quantum system only through its static part $S(0)$. Figure 6 shows the resulting purities P_1 and P_2 for the case that qubit 1 is coupled to the reservoirs R3-R4. In Figure (a) both P_1 and P_2 remain close to 1 because $S(0) \approx 0$. In Figure (b), however, $S(0) = 1$, and both systems are affected in a similar way.

IV. EXPERIMENTAL PROCEDURE AND RESULTS

A. Implementation of Hamiltonians

For the experimental implementation, we chose Carbon-13 labelled chloroform (CHCl_3) dissolved in d6-acetone as the quantum register. We chose the carbon as qubit 1 and the proton as qubit 2. The noise term in Eq. (2) is introduced by an offset variation of the transmitter on channel 2. The Hamiltonian of the two qubit NMR system is thus

$$H_{NMR,k}(t) = \frac{1}{2}\hbar\omega_z^1\sigma_z^1 + \frac{1}{2}\hbar\omega_z^2\sigma_z^2 + \frac{1}{2}\hbar\pi J\sigma_z^1\sigma_z^2 + \hbar\pi s_k(t)A, \quad (13)$$

where $A = \sigma_z^2$ or σ_z^1 and the coupling is $J = 215$ Hz.

The transverse field in Eq. (1) is applied as a radio frequency (rf) field, which can be written as

$$H_{rf} = -\frac{1}{2}\hbar\omega_x^2\sigma_x^2 \quad (14)$$

in the rotating reference frame.

In the experimental implementation, the perturbation and thus the total Hamiltonian are piecewise constant for short periods $\tau = 304.38 \mu\text{s}$. For each of these periods, we realized the total evolution $e^{-i\tau H_k(t)/\hbar}$ as $e^{-i\tau H_{NMR,k}/\hbar}e^{-i\tau H_{rf}/\hbar}$, i.e. by a short free precession period followed by a small flip-angle pulse [30]. This is a good approximation when $\tau \ll 2\pi/\omega_{nm}$.

For the experimental implementation of the reservoirs R1-R4 shown in Figure 2, we used $M = 12$ noise traces. The corresponding spectral functions are similar to those represented in Figures 2 (a-d).

The experiments start with the effective pure state $|00\rangle\langle 00|$ prepared by spatial averaging [31, 32]. The pulse sequence $[\alpha]_x^2 - [\text{grad}]_z - [\pi/4]_x^2 - \frac{1}{4J} - [\pi]_x^{1,2} - \frac{1}{4J} - [-\pi]_x^{1,2} - [-\pi/4]_y^2 - [\text{grad}]_z$ transforms the system from the equilibrium state to the effective pure state $|00\rangle\langle 00|$. Here $\alpha = \arccos(2\gamma_1/\gamma_2) \approx \pi/3$, where γ_1 and γ_2 denote the gyromagnetic ratios of ^{13}C and ^1H , respectively, and $[\text{grad}]_z$ denotes a gradient pulse along the z -axis. $\frac{1}{4J}$ denotes the evolution caused by H_{NMR} for a time $\frac{1}{4J}$. The pulses are applied from left to right. The complete pulse sequences for the implementation of the Grover search in the two systems are shown as Figures 7 (a) and (b), respectively.

B. Grover Search in systems not coupled to reservoirs

When the system is in $|00\rangle\langle 00|$, we experimentally measured the density matrix shown as Figure 8 through state tomography [33]. In either system the Grover algorithm is repeated 12 times, using different noise traces. The target state is $|11\rangle$. The final NMR signals are obtained by summing the 12 signals acquired via the readout pulse.

We first implement the Grover search in the systems without engineered noise, i.e., the noise signal $\alpha s_k(t)$ ($k = 1, 2, \dots, 12$) is not applied to the quantum systems. After the completion of the search algorithm, the density matrices of the two systems are shown as Figures 9 (a-b), respectively.

In the experiments, the imperfections of the rf pulses and natural decoherence cause errors in the search results. In order to distinguish these errors from those that are due to the engineered "noise" that we investigate here, we use the results of in Figures 9 (a-b) as the references for subsequent experiments in the systems coupled to the reservoirs. We denote these reference states as ρ_0^{I} and ρ_0^{II} .

To estimate the effects of the errors caused by imperfections of the rf pulses and natural decoherence, we compare the experimental results to simulation data, where the rf pulses are perfect and no natural decoherence exists. These results are shown as Figures 9 (c-d) corresponding to (a-b), respectively. The overlap between ρ_0 and its corresponding simulated result is 0.97 for system I and 0.91 for system II.

C. Search results in systems coupled to reservoirs

To simulate the noisy reservoir and observe the decoherence effect, we apply $M = 12$ different noise traces $\alpha s_k(t)$ to the system during the implementation of the Grover search and add the resulting signals. We quantify the resulting decoherence by the fidelity $F_\rho = \text{Tr}(\rho_0 \rho)$.

Figure 10 shows the resulting density operators for the case where the coupling operator is $A = \sigma_z^2$ and the reservoir is R1-R3. The upper row corresponds to Fig. I, the lower row to Fig. II. In all cases, the coupling strength was set to $\alpha = 63.66$ Hz. The fidelity F_ρ shown in the figures was calculated as the overlap between the states resulting from the noisy experiment and those from the experiment without the reservoir.

The observed results are in good agreement with the predictions from the numerical simulations shown in Figure 5. For example, the reduction of P_1 in Figure 5 (a) leads to the low fidelity $F_\rho = 0.69$ in Figure 10 (a), while F_ρ in Figure 10 (d) is 0.92 and P_2 in Figure 5 (a) remains close to 1. In Figures 10 (c) and (f), the fidelity in system II is larger than that in system I, in good agreement with the result that $P_2 > P_1$ in Figure 5 (c).

Figure 11 shows the search result for the case where the coupling operator is $A = \sigma_z^1$ and the systems are coupled to reservoirs R3-R4. In Figures (a) and (c), $\alpha = 63.66$ Hz; in Figures (b) and (d), $\alpha = 25.46$ Hz. The experimental results agree with the results in Figure 6. The much higher fidelity of the first column show clearly that the reservoir affects the system only through $S(0)$.

V. GENERALIZATIONS

The above description of the decoherence process uses the semiclassical approximation, where the environment interacts with the system through classical fields. The results are easily generalized to the case of a quantum mechanical environment. For this purpose, we describe the total system (quantum register plus bath) by the Hamiltonian

$$H_{tot} = H_s + H_B + H_I \quad (15)$$

where H_B denotes the Hamiltonian of the bath, and H_I denotes the coupling between the system and the bath. For the purpose of comparison we choose $H_I = AX$ where X denotes an operator of the bath.

In the quantum mechanical description, the dynamics of the quantum register are obtained by tracing over the degrees of freedom of the environment. It is thus possible to recover the Bloch- Redfield equations. In the eigenbase of H_s , the rates Λ_{lmnk} (8-10) become [18, 19]

$$\Lambda_{lmnk} = A_{lm}A_{nk} \int_0^\infty \frac{1}{\hbar^2} e^{-i\omega_{nk}t} \langle X(t)X(0) \rangle dt \quad (16)$$

where $X(t) = e^{iH_B t/\hbar} X e^{-iH_B t/\hbar}$. The brackets $\langle \dots \rangle$ denote the thermal average over the bath degrees of freedom. The Fourier transform of this correlation function corresponds to the spectral function $S(\omega_{nk})$ in Eq. (10). This means that the fully quantum model described by Eq. (15) can be mapped to the quantum system under classical noise described by Eq.

(2) [28]. Consequently our results are equally applicable to the fully quantum-mechanical case.

Besides the coupling between the quantum system and its environment, pulse imperfections (i.e. nonideal gate operations) also induce decoherence. Our results can be easily generalized to investigate the effect of the pulse imperfections on the decoherence rate. The generalization is illustrated by rewriting Eq. (2) as

$$H(t) = \frac{1}{2}\hbar \left[\Omega_z^1(t)\sigma_z^1 + \omega_z^2\sigma_z^2 - \omega_x^2\sigma_x^2 + \pi J\sigma_z^1\sigma_z^2 \right] \quad (17)$$

where $\Omega_z^1(t) = \omega_z^1 + 2\pi s(t)$, when $A = \sigma_z^1$. $\Omega_z^1(t)$ denotes the strength of the pulse that randomly fluctuates about ω_z^1 , and $2\pi s(t)$ describes the fluctuation. Using our methods, one can discuss the effects of different fluctuations and search for experimental conditions that minimize the effect of pulse imperfections.

VI. CONCLUSION

We have investigated, experimentally and theoretically, the effect of different reservoirs on the decoherence of quantum registers during the execution of a quantum algorithm. While we have used a semiclassical system for these investigations, the results are easily adapted to a quantum mechanical environment, such as a spin-boson model.

The system Hamiltonian as well as the coupling operator determine whether the environment causes pure dephasing or also induces transitions. The situation that is probably most relevant for quantum information processing is the case where the coupling operator is diagonal in the eigenbase of the system Hamiltonian. In this case, the environment causes pure dephasing and only the static part of the perturbation, $\propto |S(0)|$ causes decoherence.

While we have chosen a 2-qubit system for this investigation, the results are completely general and can be applied directly to multi-qubit systems. It is possible to use this method of simulating dissipative quantum systems for related phenomena, such as dissipative quantum phase transitions [34]. In the field of quantum information processing, our results indicate possible ways for suppressing decoherence.

VII. ACKNOWLEDGMENT

We thank Prof. Jiangfeng Du and Dr. Bo Chong for helpful discussions. The experiments were performed at the Interdisciplinary Center for Magnetic Resonance. This work is supported by the Alexander von Humboldt Foundation, the National Natural Science Foundation of China under grant No. 10374010, the DFG through Su 192/19-1, and the Graduiertenkolleg No. 726.

- [1] W. G. Unruh, Phys. Rev. A **51**, 992 (1995)
- [2] D. P. DiVincenzo, Science, **270**, 255 (1995); I. L. Chuang, R. Laflamme, P. W. Shor, W. H. Zurek, *ibid.* **270**, 1633 (1995); C. H. Bennett and D. P. DiVincenzo, Nature, **404**, 247 (2000); W. H. Zurek, Rev. Mod. Phys, **75**, 715 (2003); M. Schlosshauer, *ibid.* **76**, 1267 (2004)
- [3] P. W. Shor, Phys. Rev. A **52**, R2493 (1995); D. Gottesman, *ibid.* **54**, 1862 (1996); A. M. Steane, *ibid.* **54**, 4741 (1996); E. Knill and R. Laflamme, *ibid.* **55**, 900 (1997); D. P. DiVincenzo¹ and P. W. Shor, Phys. Rev. Lett. **77**, 3260 (1996); R. Laflamme, C. Miquel, J. P. Paz, and W. H. Zurek, *ibid.* **77**, 198 (1996); J. Preskill, Proc. R. Soc. Lond. A **454**, 385 (1998)
- [4] L. Viola, E. Knill, and S. Lloyd, Phys. Rev. Lett. **82**, 2417 (1999); L. Viola, S. Lloyd, and E. Knill, *ibid.* **83**, 4888 (1999); L. Viola, and E. Knill, *ibid.* **90**, 037901 (2003); **94**, 060502 (2005); O. Kern, and G. Alber, *ibid.* **95**, 250501 (2005); K. Khodjasteh, and D. A. Lidar, *ibid.* **95**, 180501 (2005); L. Viola, Phys. Rev. A **66**, 012307 (2002); L. Viola, S. Lloyd, *ibid.* **58**, 2733 (1998); K. Shiokawa and D. A. Lidar, *ibid.* **69**, 030302(R) (2004); P. Zanardi, Phys. Lett. A **258**, 77 (1999)
- [5] P. Zanardi, and M. Rasetti, Phys. Lett. A **264**, 94 (1999); Phys. Rev. Lett. **79**, 3306 (1997); L.-M. Duan, and G.-C. Guo, *ibid.* **79**, 1953 (1997); D. A. Lidar, I. L. Chuang, and K. B. Whaley, *ibid.* **81**, 2594 (1998)
- [6] L.-M. Duan, J. I. Cirac, P. Zoller, Science, **292**, 1695 (2001); J. Pachos, P. Zanardi, and M. Rasetti, Phys. Rev. A **61**, 010305(R) (1999); S.-L. Zhu and P. Zanardi, *ibid.* **72**, 020301(R) (2005); L.-A. Wu, P. Zanardi, and D. A. Lidar, Phys. Rev. Lett. **95**, 130501 (2005)
- [7] B. Misra and E. C. G. Sudarshan, J. Math. Phys. **18**, 756 (1977); W. Hwang, H. Lee, D. Ahn, and S. W. Hwang, Phys. Rev. A **62**, 062305 (2000); R. Filip, *ibid.* **67**, 014308 (2003);

- P. Facchi, D. A. Lidar, and S. Pascazio, *ibid.* **69**, 032314 (2004); O. Hosten, M. T. Rakher, J. T. Barreiro, N. A. Peters, and P. G. Kwiat, *Nature*, **439**, 949 (2006); D. Dhar, L. K. Grover, and S. M. Roy, *Phys. Rev. Lett.* **96**, 100405 (2006)
- [8] I. A. Grigorenko and D.V. Khveshchenko, *Phys. Rev. Lett.* **94**, 040506 (2005)
- [9] I. A. Grigorenko and D.V. Khveshchenko, *Phys. Rev. Lett.* **95**, 110501 (2005)
- [10] E. Knill, R. Laflamme, and L. Viola, *Phys. Rev. Lett.* **84**, 2525 (2000); P. Zanardi and S. Lloyd, *ibid.* **90**, 067902 (2003)
- [11] P. Facchi, D. A. Lidar, and S. Pascazio, *Phys. Rev. A* **69**, 032314 (2004)
- [12] D. G. Cory, M. D. Price, W. Maas, E. Knill, R. Laflamme, W. H. Zurek, T. F. Havel, and S. S. Somaroo, *Phys. Rev. Lett.* **81**, 2152 (1998); E. Knill, R. Laflamme, R. Martinez, and C. Negrevergne, *ibid.* **86**, 5811 (2001)
- [13] L. Viola, E. M. Fortunato, M. A. Pravia, E. Knill, R. Laflamme, D. G. Cory, *Science*, **293**, 2059 (2001); E. M. Fortunato, L. Viola, M. A. Pravia, E. Knill, R. Laflamme, T. F. Havel, and D. G. Cory, *Phys. Rev. A* **67**, 062303 (2003); D.-X. Wei, J. Luo, X.-P. Sun, X.-Z. Zeng, M.-S. Zhan, and M.-L. Liu, *Phys. Rev. Lett.* **95**, 020501 (2005); J. E. Ollerenshaw, D. A. Lidar, and L. E. Kay, *ibid.* **91**, 217904 (2003)
- [14] J. A. Jones, V. Vedral, A. Ekert, G. Castagnoli, *Nature*, **403**, 869 (2000); J.-F. Du, P. Zou, M.-J. Shi, L.-C. Kwek, J.-W. Pan, C. H. Oh, A. Ekert, D. K. L. Oi, and M. Ericsson, *Phys. Rev. Lett.* **91**, 100403 (2003)
- [15] Y. Kondon, M. Nakahara, and S. Tanimura, arXiv: quant-ph/0604112
- [16] N. V. Prokof'ev and P. C. E. Stamp, *Rep. Prog. Phys.* **63**, 669 (2000)
- [17] U. Weiss, *Quantum dissipative systems*, 2nd ed. (World Scientific, Singapore, 1999); A. J. Leggett, S. Chakravarty, A. T. Dorsey, M. P. A. Fisher, A. Garg, and W. Zwerger, *Rev. Mod. Phys.* **59**, 1 (1987); Y. Makhlin, G. Schön, A. Shnirman, *ibid.* **73**, 357 (2001); G.-L. Ingold, *Path integrals and their application to dissipative quantum systems*, to be published in "Coherent Evolution in Noisy Environments", Lecture Notes in Physics, Springer Verlag, Berlin-Heidelberg-New York; F. K. Wilhelm, S. Kleff, and J. von Delft, *Chem. Phys.* **296**, 345 (2004); C.-P. Sun, and L.-H. Yu, *Phys. Rev. A* **51**, 1845 (1995); M. Thorwart, and P. Hänggi, *ibid.* **65**, 012309 (2001); H. Jirari and W. Pötz, *ibid.* **74**, 022306 (2006)
- [18] M. J. Storcz and F. K. Wilhelm, *Phys. Rev. A* **67**, 042319 (2003); M. Governale, M. Grifoni, and G. Schön, *Chem. Phys.* **268**, 273 (2001)

- [19] M. J. Storcz, F. Hellmann, C. Hrelescu, and F. K. Wilhelm, Phys. Rev. A **72**, 052314 (2005)
- [20] K. M. Fonseca-Romero, S. Kohler, and P. Hänggi, Phys. Rev. Lett. **95**, 140502 (2005); S. Kohler, and P. Hänggi, e-print: quant-ph/0509085
- [21] G. Teklemariam, E. M. Fortunato, C. C. López, J. Emerson, J. P. Paz, T. F. Havel, and D. G. Cory, Phys. Rev. A **67**, 062316 (2003)
- [22] M. Laforest, D. Simon, J.-C. Boileau, J. Baugh, M. J. Ditty, and R. Laflamme, Phys. Rev. A **75**, 012331 (2007)
- [23] L. K. Grover, Phys. Rev. Lett. **79**, 325 (1997); *ibid.* **80**, 4329 (1998); *ibid.* **95**, 150501 (2005)
- [24] I. L. Chuang, N. Gershenfeld, and M. Kubinec, Phys. Rev. Lett. **80**, 3408 (1998); J.-F. Zhang, Z.-H. Lu, L. Shan, and Z.-W. Deng, Phys. Rev. A **65**, 034301 (2002); L. Xiao and J. A. Jones, *ibid.* **72**, 032326 (2005); J. Åberg, D. Kult, and E. Sjöqvist, *ibid.* **71**, 060312(R) (2005); J. Ahn, T. C. Weinacht, P. H. Bucksbaum, Science, **287**, 463 (2000); P. G. Kwiat, J. R. Mitchell, P. D. D. Schwindt, and A. G. White, J. Mod. Opt. **47**, 257 (2000), also seeing quant-ph/9905086; P. Walther, K. J. Resch, T. Rudolph, E. Schenck, H. Weinfurter, V. Vedral, M. Aspelmeyer, and A. Zeilinger, Nature, **434**, 169 (2005); J. A. Jones, M. Mosca, and R. H. Hansen, *ibid.* **393**, 344 (1998); A. Mitra, A. Ghosh, R. Das, A. Patel and A. Kumar, J. Magn. Reson. **177**, 285 (2005)
- [25] A. Abragam, *The Principles of Nuclear Magnetism* (Oxford University Press, New York, 1961); S. Dattagupta, *Relaxation phenomena in condensed matter physics*, Academic press, INC (1987: Florida)
- [26] J. A. Jones, Phys. Rev. A **67**, 012317 (2003)
- [27] G. M. Palma, K.-A. Suominen, and A. K. Ekert, Proc. R. Soc. Lond. A **452**, 567 (1996)
- [28] O.-P. Saira, V. Bergholm, T. Ojanen, and M. Möttönen, Phys. Rev. A **75**, 012308 (2007)
- [29] J. F. Poyatos, J. I. Cirac, and P. Zoller, Phys. Rev. Lett. **78**, 390 (1997)
- [30] L. M. K. Vandersypen, and I. L. Chuang, **76**, Rev. Mod. Phys. **76**, 1037(2004); X.-H. Peng, J.-F. Du, and D. Suter, Phys. Rev. A **71**, 012307 (2005)
- [31] D. G. Cory, M. D. Price, and T. F. Havel, Physica D, **120**, 82 (1998)
- [32] J.-F. Du, T. Durt, P. Zou, H. Li, L. C. Kwek, C. H. Lai, C. H. Oh, and A. Ekert, Phys. Rev. Lett. **94**, 040505 (2005); X.-H. Peng, X.-W. Zhu, D. Suter, J.-F. Du, M.-L. Liu, and K.-L. Gao, Phys. Rev. A **72**, 052109 (2005); J.-F. Zhang, Z.-H. Lu, L. Shan, and Z.-W. Deng, *ibid.* **66**, 044308 (2002)

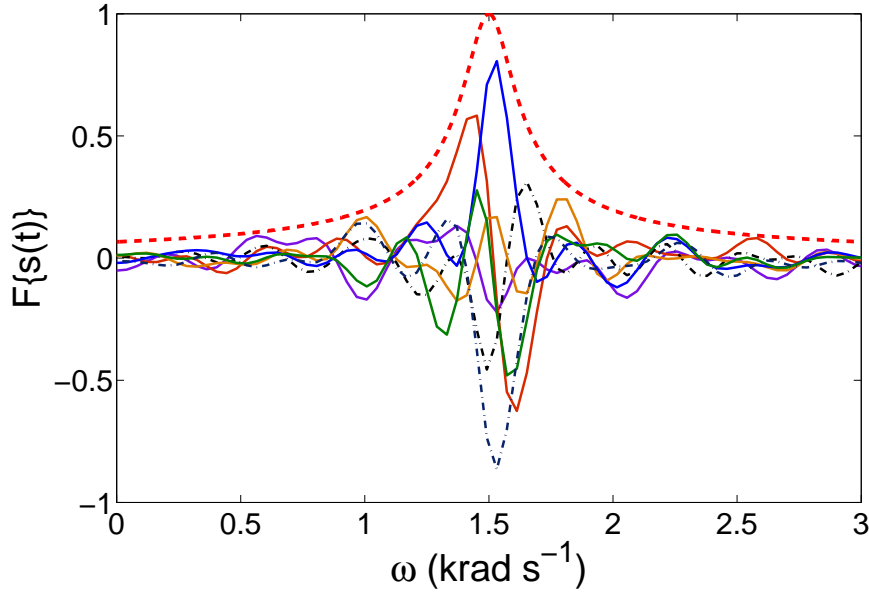


FIG. 1: (Color online) Spectra (solid and dot dashed curves) of some random functions $s(t)$. The dashed curve represents the envelope function $\sqrt{S(\omega)}$.

- [33] I. L. Chuang, N. Gershenfeld, M. G. Kubinec, and D. W. Leung, Proc. R. Soc. London, Ser. A **454**, 447 (1998); G. M. Leskowitz and L. J. Mueller, Phys. Rev. A **69**, 052302 (2004)
- [34] A. J. Bray, and M. A. Moore, Phys. Rev. Lett. **49**, 1545 (1982); S. Chakravarty, G.-L. Ingold, S. Kivelson, and A. Luther, *ibid.* **56**, 2303 (1986); L. Capriotti, A. Cuccoli, A. Fubini, V. Tognetti, and R. Vaia, *ibid.* **94**, 157001 (2005); A. Kapitulnik, N. Mason, S. A. Kivelson, and S. Chakravarty, Phys. Rev. B **63**, 125322 (2001); T. Stauber and F. Guinea, Phys. Rev. A **73**, 042110 (2006)

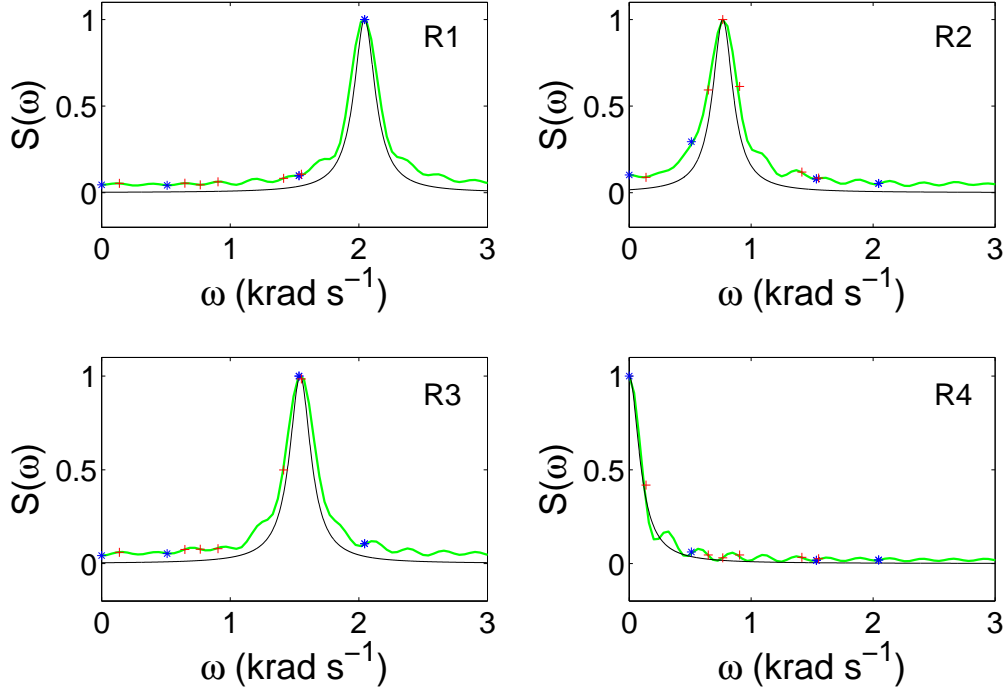


FIG. 2: (Color online) Normalized spectral functions for the four reservoirs (R1-R4) with $\Gamma = 100 \text{ s}^{-1}$ and $\omega_0 = \omega_{42}^I$, ω_{32}^{II} , $(\omega_{31}^I + \omega_{41}^{II})/2 \approx \omega_{31}^I \approx \omega_{41}^{II}$ and 0, respectively. The thick curves represent the generated spectral functions for each reservoir, which were generated by averaging over 2500 noise signals. The thin curves represent the corresponding theoretical spectral functions. The transition angular frequencies of the systems I and II are marked by "*" and "+".

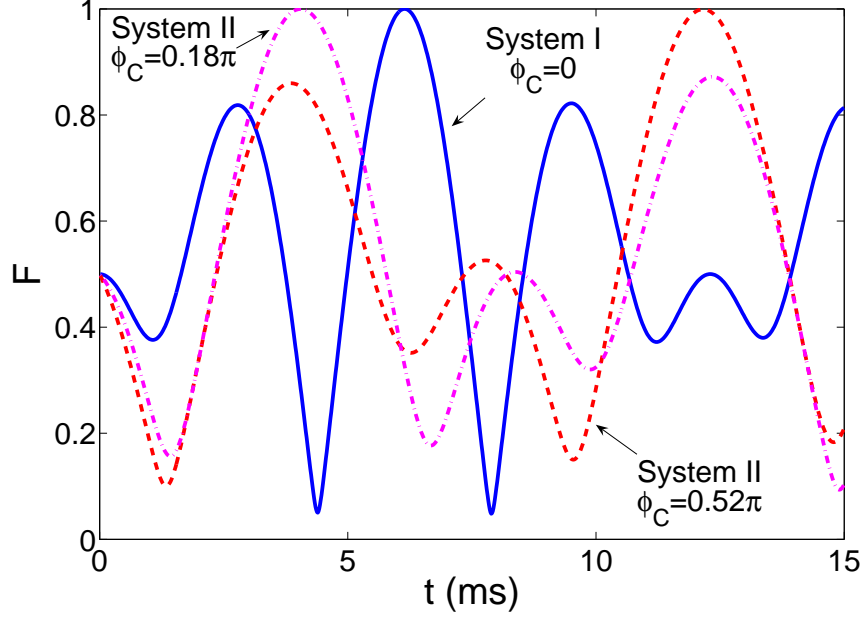


FIG. 3: (Color online) Time dependence of the fidelity for the CNOT-equivalent operation. In system I, shown as the solid curve, the proper evolution time is 6.15 ms, and $\phi_C = 0$. In system II, shown as the dash-dotted and dashed curves, the proper evolution times are 4.05 ms and 12.18 ms for $\phi_C = 0.18\pi$ and 0.52π , respectively.

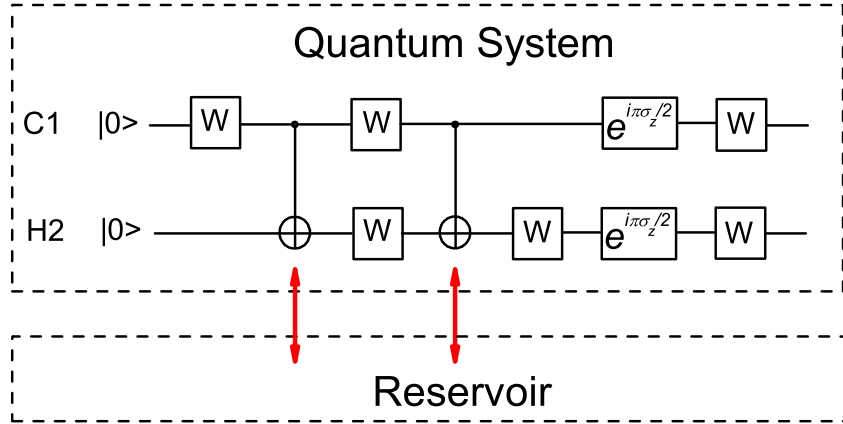


FIG. 4: (Color online) Gate sequence for the Grover search in an open quantum system. The time order is from left to right. W denotes the Walsh-Hadamard transform, and the red arrows denote the interaction between the system and reservoir. The duration of the gates W and $e^{i\pi\sigma_z/2}$ is so short that it can be ignored.

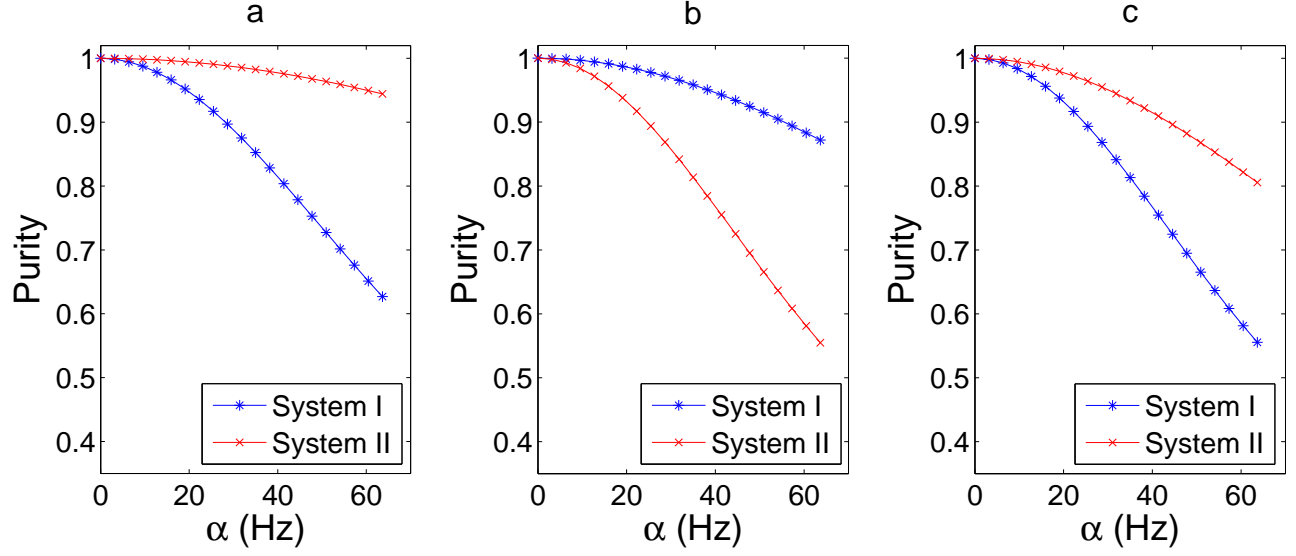


FIG. 5: (Color online) Purity of Grover search process as a function of the coupling strength to the environment when qubit 2 is coupled to the reservoirs in R1-R3, respectively. The data points obtained in systems I and II are marked by "*" and "x", respectively.

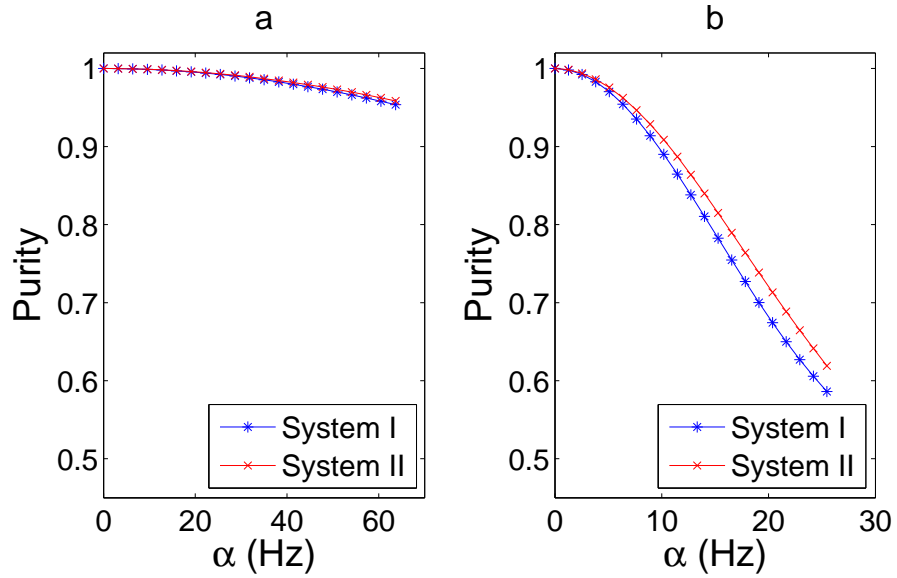


FIG. 6: (Color online) Same as Fig. 5, but for qubit 1 coupled to reservoirs R3-R4.

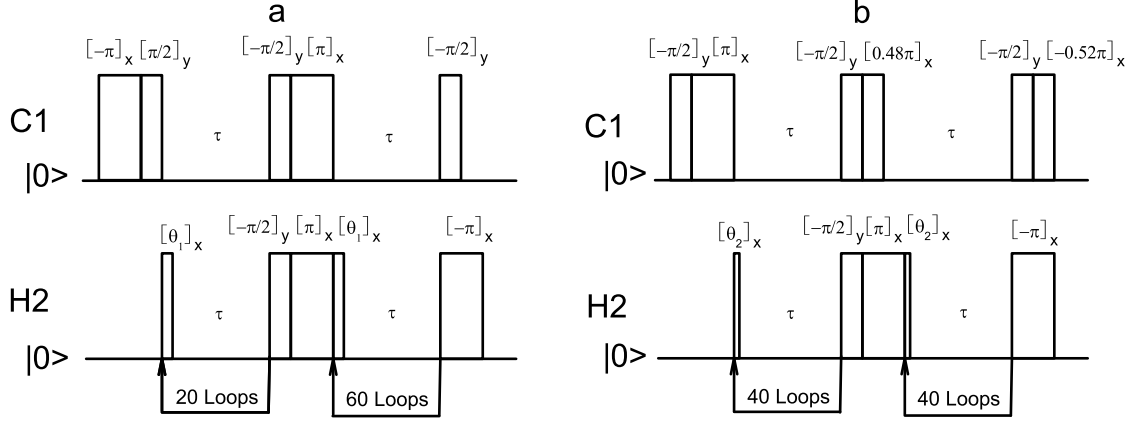


FIG. 7: Pulse sequences to implement the Grover search in systems I shown in (a) and II shown in (b). The flip angles θ_1 and θ_2 for the two systems differ by a factor of 2. During the delay denoted by τ , the systems evolve under the natural Hamiltonian and the noise signal of Eq. (13).

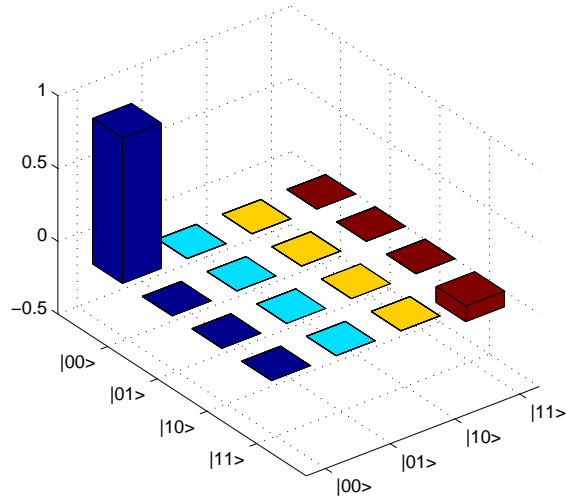


FIG. 8: (Color online) Experimentally measured density matrix when the system lies in the initial pseudo-pure state $|00\rangle\langle 00|$.

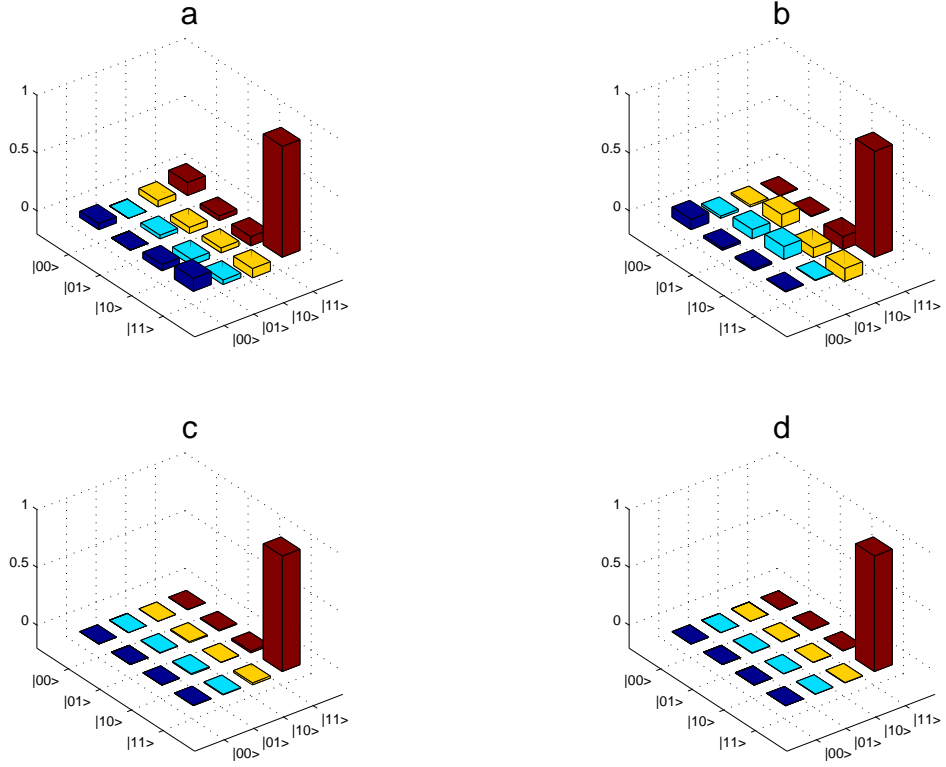


FIG. 9: (Color online) Experimentally measured density matrices after the completion of the Grover search in the systems I [shown as (a)], and II [shown as (b)] when the reservoir is not applied. The target state is chosen as $|11\rangle$. The matrices have been normalized. Only the real parts of the elements are plotted. The imaginary parts are less than 18%. In order to estimate the errors caused by the imperfections of rf pulses and natural decoherence, Figures (c-d) show the simulated results obtained by NMR simulator where the rf pulses are perfect and no natural decoherence exists, corresponding to Figures (a-b), respectively.

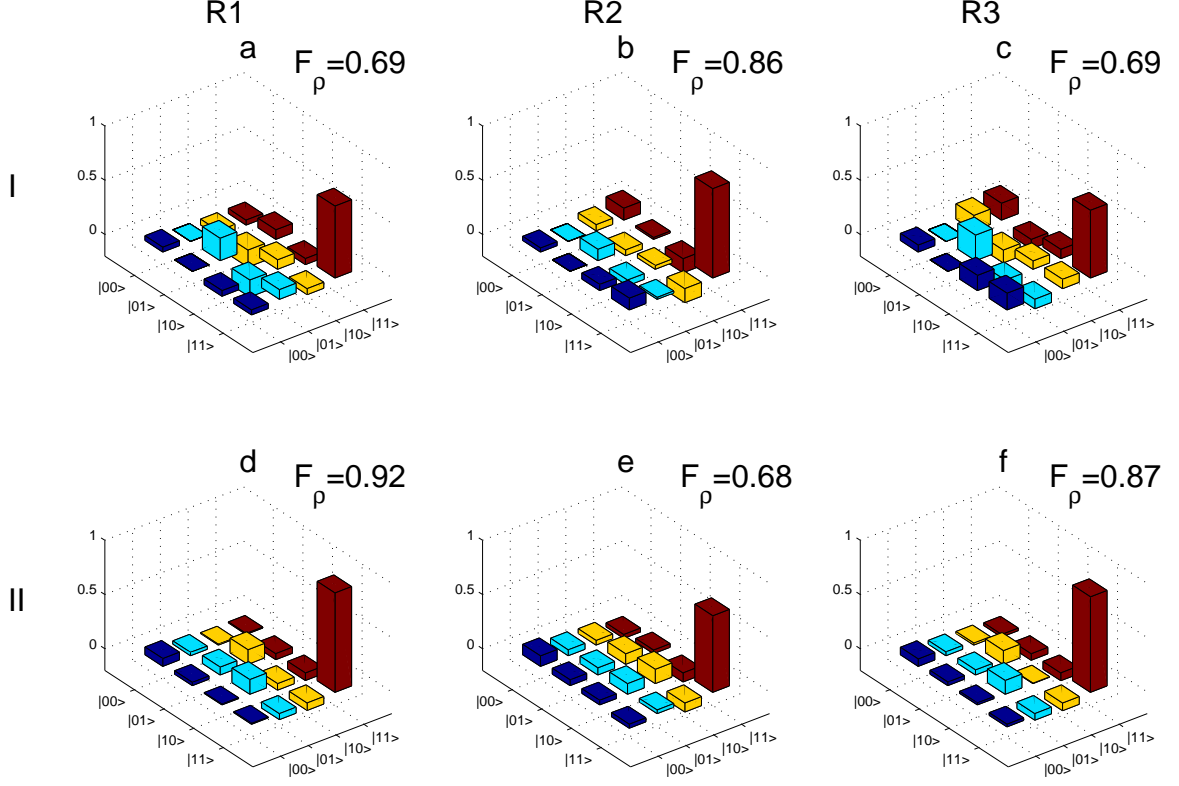


FIG. 10: (Color online) Experimentally measured density matrices after the completion of the Grover search when qubit 2 is coupled to reservoirs R1-R3, shown as the three columns from left to right. The two rows of figures show the results obtained in systems I and II, respectively. F_ρ denotes the fidelity of the search result with respect to the corresponding noiseless result.

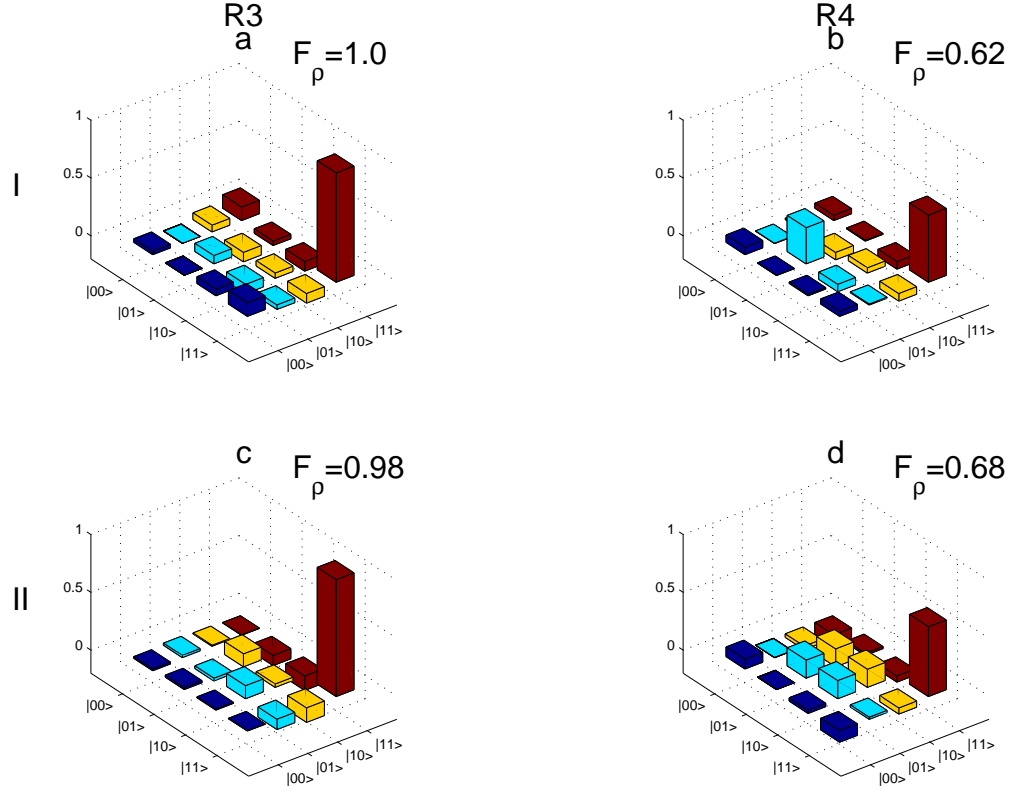


FIG. 11: (Color online) Experimentally measured density matrices after the completion of the Grover search when qubit 1 is coupled to reservoirs R3-R4, shown as the two columns from left to right.